Structural and electronic properties of lutecia from first principles

2009 J. Phys.: Condens. Matter 21 455601

(http://iopscience.iop.org/0953-8984/21/45/455601)

J. Phys.: Condens. Matter **21** (2009) 455601 (7pp) doi:10.1088/0953-8984/21/45/455601

Structural and electronic properties of lutecia from first principles

Lixin Ning[1,3], **Yongfan Zhang**[2] **and Zhifeng Cui**[1]

[1] Department of Physics, Anhui Normal University, Wuhu, Anhui 241000, People's Republic of China
[2] Department of Chemistry, Fuzhou University, Fuzhou, Fujian 350002, People's Republic of China

E-mail: ninglx@mail.ahnu.edu.cn

Received 7 July 2009, in final form 7 October 2009
Published 23 October 2009
Online at stacks.iop.org/JPhysCM/21/455601

Abstract

The structural and electronic properties of lutecia (C-type Lu_2O_3) have been investigated using the projected augmented wave (PAW) method based on the periodic density functional theory (DFT). Two models for the localized Lu 4f electrons have been employed, in which the f electrons are treated as a part of the inner core and as valence electrons, respectively. With the former model, the Perdew–Burke–Ernzerhof (PBE) calculations yield a crystal structure in good agreement with experiments, while with the latter model, the PBE + U results show that the optimum U_{eff} parameter value is dependent on the property investigated. The variation of structural properties with respect to the model used and the U_{eff} value chosen has been rationalized in terms of the repulsive interaction between Lu 4f and O 2p electrons owing to the insufficient self-interaction cancelation associated with the localized f electrons in the DFT functional. Based on the calculated results, a practical scheme is proposed for the calculation of Lu_2O_3 and the related materials in cases where the f electronic properties are relevant.

(Some figures in this article are in colour only in the electronic version)

1. Introduction

The C-type Lu_2O_3 crystal has received considerable interest due to its characteristic properties, such as good thermal and phase stabilities, low phonon energy, ease of doping with other lanthanide ions, and optical transparency from near-infrared to visible regions [1–8]. These properties are very favorable for applications in optical devices, e.g., in lighting, displays, and x-ray detection. This material has also been considered as a promising candidate for replacing the conventional silicon dioxide as a gate dielectric in metal-oxide-semiconductor (MOS) nanoelectronic devices, owing to its high dielectric constant (around 12) and the expected thermodynamical stability on silicon [9, 10]. In this type of application, the band alignment of the dielectric material with the semiconductor substrate strongly affects the reliability of the MOS devices, usually requiring a valence band offset of higher than 1 eV. This band offset is quite difficult to determine experimentally, for example, by x-ray photoelectron spectroscopy (XPS), due to the complexity of the electronic configuration. Since the valence band structure of Lu_2O_3 near the Fermi level is partially determined by the Lu 4f electrons, which have a higher cross section in the XPS spectrum than the outer valence electrons, the information of the 4f band position relative to the Fermi level may be used to determine the valence band offset and thus the reliability of the MOS devices.

Systems containing 4f-block elements present a challenge for electronic band theory due to the correlated character of the localized 4f orbitals. For Lu_2O_3, one might expect this is not a problem if one is only concerned with the crystal structure, because the 4f shell of lutetium is complete and thus the electronic correlation could be neglected. Indeed, such calculations have been reported on the structure of this material by keeping the 4f electrons frozen in the core [11, 12]. However, as referred to above, cases exist in which the 4f electronic properties play an important role [9, 10]. It would therefore be desirable to study the crystal from first principles by treating the 4f electrons in the valence states. Unfortunately, to the best of our knowledge no such study has been reported on Lu_2O_3. This lack is not wholly accidental, since besides the

[3] Author to whom any correspondence should be addressed.

theoretical complexity of the compact and completely filled 4f shell, lutecia has a complicated crystal structure with 16 Lu_2O_3 formulae (80 atoms) per unit cell, the calculation of which is computational demanding.

The local density (LDA) or generalized-gradient (GGA) approximations to the exchange–correlation functional in DFT are often unable to reproduce the electronic properties of materials with strongly localized 4f electrons. The main reason is the incomplete cancelation of the Coulomb self-interaction in these functionals, which favors delocalized solutions. Different approaches have been developed to overcome this problem. One approach is to include some portion of HF exchange in the DFT functional (referred as hybrid functionals), which has been successfully applied to the study of ceria and related materials [13, 14]. Another way to address the problem is to use the so-called DFT + U approach, in which a Hubbard-like Hamiltonian is introduced to remedy the strong on-site Coulomb repulsion among the localized electrons [15–17]. This approach may be understood as introducing an energy penalty to the DFT total energy for fractional populations, thus disfavoring delocalization of atomic-like orbitals. It corrects most of the inadequacies of the DFT treatment for localized states, although the choice of the interaction strength U is uncertain in the sense that it strongly affects the calculated results. It is usually chosen to optimize agreement with experiments. DFT + U applications on cerium oxides and praseodymium dioxide have been reported, with very satisfactory results obtained [18–22]. Finally, we mention the self-interaction corrected local spin density approach (SIC-LSDA) which has been used to reduce the hybridization of states of localized electrons with the valence band [23].

In the present work, we report DFT calculations on the structural and electronic properties of the C-type Lu_2O_3 using two models for the localized Lu 4f electrons, in which the f electrons are treated as a part of the inner core and as valence electrons, respectively. In the latter model, the DFT + U methodology has been employed to describe the f electrons and the importance of the on-site Lu 4f electronic correlation represented by the U_{eff} parameter has been investigated. The choice of this methodology over others such as hybrid functionals is due to the large size of the system under investigation. The main motivation for this study is to analyze the response of the structural and electronic properties of Lu_2O_3 to various descriptions for the completely filled Lu 4f shell and to see whether these properties can be predicted in a consistent way. This paper is organized as follows. The computational method and details are described in section 2, and the calculated results are presented and discussed in section 3. The final conclusions are collected in section 4.

2. Computational methods

All DFT calculations were carried out using the Vienna *ab initio* simulation package (VASP) [24], where the basis set is constructed from plane waves. The interaction between the valence electrons and the core is described using the PAW method [25] in the implementation of Kresse and Joubert [26]. The PBE functional [27] has been employed together with its PBE + U variant. The 5s, 5p, 5d, 4f, and 6s states on Lu were included in the valence basis when the 4f electrons were treated as valence electrons, while only 5p, 5d, and 6s states were explicitly considered when the 4f electrons are treated as part of the inner core. For the O atom the 2s and 2p orbitals were taken as valence states. The optimizations of structures were conducted via a conjugate gradient technique, which uses the total energy and Hellmann–Feynman forces on the atoms as convergence criteria. The internal parameters were relaxed at constant cell volume until the total forces on each ion were less then 0.02 eV Å^{-1}. In the total energy calculation, the blocked Davidson-like algorithm was selected for electronic minimization with the criterion of 10^{-6} eV. To ensure converged results, the cutoff energy for the plain wave basis was set as 400 eV and the Monkhorst–Pack scheme based on $3 \times 3 \times 3$ k-point grid (14 irreducible k points) was used to sample the Brillouin zone.

In the DFT + U approach, the standard PBE energy functional is supplemented with a Hubbard-like Hamiltonian to correct the strong on-site Coulomb repulsion among the localized Lu 4f electrons. In this work, the rotationally invariant formalism by Dudarev *et al* [28] was adopted,

$$E_{\text{PBE}+U} = E_{\text{PBE}} + \frac{U_{\text{eff}}}{2} \sum_{\sigma} \text{Tr}\,[\rho^{\sigma} - \rho^{\sigma}\rho^{\sigma}]$$

where ρ is the 7×7 density matrix of the 4f states, and σ denotes one of two spin directions. The magnitude of the correction for the on-site Coulomb repulsion depends on the parameter $U_{\text{eff}} = U - J$, where U is a parameter representing the energy increase for an extra electron on a particular site and J is a parameter describing the screened exchange energy. Since the density matrices are idempotent for a completed full or empty band, this formalism can be understood as introducing a penalty to the PBE total energy for fractional populations (when $U_{\text{eff}} > 0$) and thus disfavoring delocalization of 4f orbitals. The corresponding effective one-electron potential is given by

$$V_{ij}^{\sigma} = \frac{\delta E_{\text{PBE}}}{\delta \rho_{ij}^{\sigma}} + U_{\text{eff}} \left[\frac{1}{2}\delta_{ij} - \rho_{ij}^{\sigma} \right]$$

when $U_{\text{eff}} > 0$, the energy of the occupied 4f-like state are lowered by about $-U_{\text{eff}}/2$ thus reducing the mixing with ligand orbitals. The $U_{\text{eff}} = 0$ eV case represents the PBE limit. The application of the plane wave DFT methodology in VASP code has recently been described in detail by Hafner [29].

3. Results and discussion

The Lu_2O_3 lattice has the cubic bixbyite structure (space group *Ia3* (*Th7*, no. 206)), with 16 Lu_2O_3 formula per unit cell. This is the only polymorphic form for lutetium sesquioxide, whereas, for the other lanthanide sesquioxides, more than one form exists. The crystal structure is sketched in figure 1. The unit cell contains 32 Lu atoms with 24 at C_2 symmetry sites and the other eight at C_{3i} sites. The Lu atoms are each 6-fold coordinated by the oxygen atom, which itself is 4-fold coordinated by one Lu atom at C_{3i} site and three Lu atoms at C_2 sites. The lattice constant is 10.391 Å [1]. The Lu(C_{3i})

Table 1. Calculated equilibrium lattice constant a, bulk modulus B, and internal parameters for the C-type Lu_2O_3 crystal. Experimental data for the C-type Lu_2O_3 and Yb_2O_3 crystals are included for comparison.

				Ln (at C_2 sites)	O (at C_1 sites)		
	Method	a (Å)	B (GPa)	$-u$	x	y	z
Lu_2O_3	CSM	10.368	154.2	0.033	0.391	0.152	0.380
	VSM						
	$U_{\text{eff}} = 0$ eV	10.478	145.1	0.033	0.391	0.152	0.380
	5 eV	10.259	148.7				
	8 eV	9.875	110.1				
	Expt.	10.391	139.7				
Yb_2O_3	Expt.	10.434		0.032–0.034	0.391–0.392	0.151–0.154	0.380–0.381

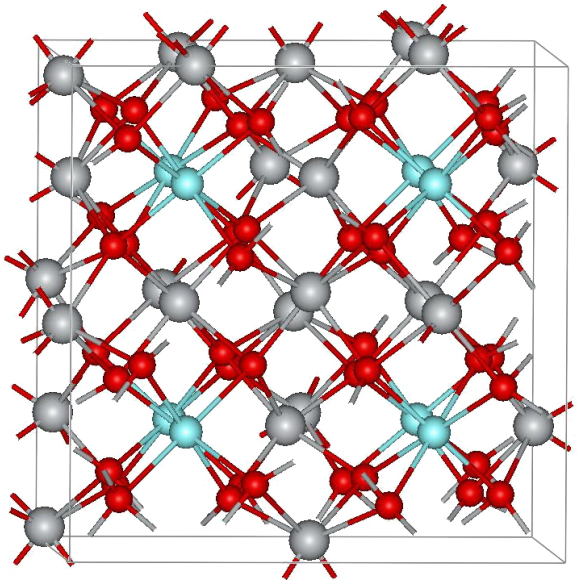

Figure 1. Crystal structure of Lu_2O_3 viewed in a direction slightly deviated from [001]. The large (gray) ball is for Lu atoms at C_2 sites, the intermediate (cyan) ball is for Lu at C_{3i} sites and the small (red) ball is for O at C_1 sites.

atoms are at fixed positions whereas the Lu(C_2) and O(C_1) sublattices are distorted depending on one and three internal parameters, respectively (see table 1). The experimental values of these internal parameters are not yet available, although in other bixbyite oxides the analogous parameters have been determined from x-ray and neutron diffraction and perturbed angular correlation techniques [30]. In the present investigation the structural and electronic properties are studied using two models for the Lu 4f electrons. The first one treats the f electrons as a part of the (chemically inert) inner core, and the second treats the f electrons explicitly in the valence states. For simplicity, we will refer to these two models as the core state model (CSM) and the valence state model (VSM), respectively.

3.1. Structural properties

The lattice constants and the bulk modulus were obtained by fitting the total energy versus cell volume curves to the Birch–Murnaghan equation of state [31, 32]. For the CSM and the VSM with $U_{\text{eff}} = 0$ eV, the total energy for each cell volume was derived with the atomic positions fully relaxed, while for the cases of VSM with $U_{\text{eff}} > 0$ eV, the internal parameters were fixed to the values predicted by the VSM with $U_{\text{eff}} = 0$ eV. The obtained structural properties in the framework of the two models are listed in table 1. One can see that, within the CSM, the PBE calculation gives an equilibrium lattice constant of 10.368 Å, which is only 0.023 Å shorter than the experimental value of 10.391 Å. When the 4f electrons are treated in the valence state (VSM), the PBE (with $U_{\text{eff}} = 0$ eV) calculation yields a value of 10.478 Å, which is 0.087 Å too long compared to experiment. With the increase of the Hubbard on-site Coulomb repulsion, the lattice constant decreases, down to a value of 9.875 Å at $U_{\text{eff}} = 8$ eV. We note a recent CSM calculation by Hirosaki *et al* [12] on the same crystal which gave a lattice constant of 10.358 Å, slightly shorter (by 0.01 Å) than our CSM value. This small discrepancy may be due to the fact that they employed the PW91 functional and a $1 \times 1 \times 1$ Monkhorst–Pack k-point grid in their calculations, whereas in the present calculation we used the PBE functional and a larger $3 \times 3 \times 3$ Monkhorst–Pack k-point grid.

Calculated values for the internal structural parameter of Lu_2O_3 from the VSM are almost identical to those from the CSM, see table 1. These values are compared with the experimental ones for the C-type Yb_2O_3, which has a lattice constant (10.434 Å) closest to that of Lu_2O_3 among the C-type lanthanide sesquioxides. This is presumably due to the similar ionic radii of the Lu^{3+} and Yb^{3+} ions in the six-fold coordination (0.861 versus 0.868 Å). We see that the obtained internal parameter values for Lu_2O_3 fall well within the experimental ranges given for Yb_2O_3. Table 1 also summarizes calculated values for the bulk modulus of Lu_2O_3. Experimentally, only one value of 139.7 GPa from the room-temperature sonic resonance measurement is available for comparison [33]. The CSM and VSM ($U_{\text{eff}} = 0$ eV) values are respectively 14.5 and 5.4 GPa larger than the experimental one.

Figure 2 shows the variation of lattice constant and bulk modulus with increasing U_{eff} in the range of 0–8 eV. It shows that the lattice constant varies over a wide range of 0.603 Å. With increasing U_{eff}, the lattice constant decreases monotonically; the behavior becoming dramatic when $U_{\text{eff}} \geqslant 6$ eV. Since the lattice constant a is overestimated (by 0.087 Å) at the pure PBE level ($U_{\text{eff}} = 0$ eV), the increase of U_{eff} makes the deviation smaller, and at $U_{\text{eff}} \sim 2.5$ eV the experimental value is matched. Also noted is that at $U_{\text{eff}} \sim 3.0$ eV the CSM

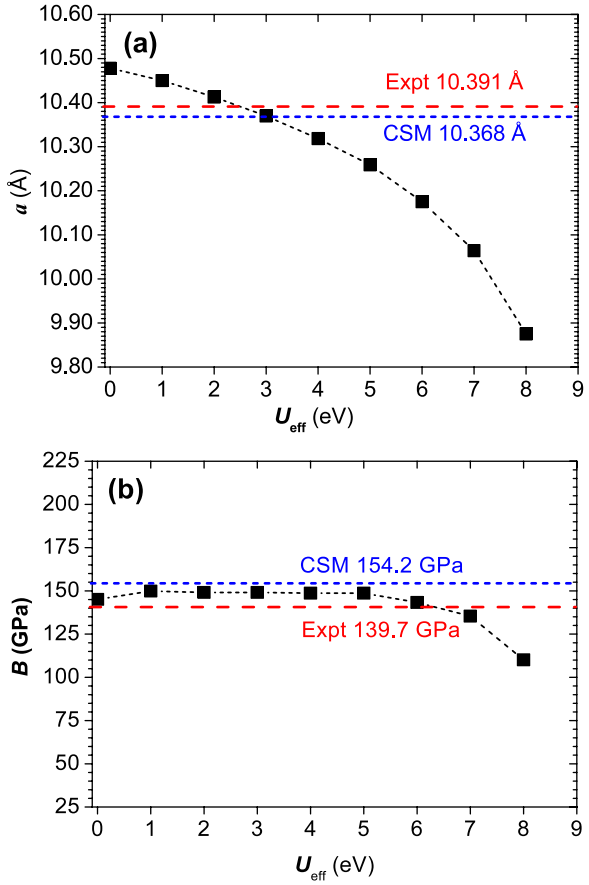

Figure 2. Variations of the calculated equilibrium lattice constant a (a) and bulk modulus B (b) of Lu_2O_3 with respect to the value of U_{eff} in the range of 0–8 eV. The results from experiments and CSM calculations are also shown for comparison.

value of 10.368 Å is reached by the VSM calculation. These data clearly demonstrate the importance of the Hubbard on-site term in the determination of the structure of Lu_2O_3 when the f states are treated explicitly in the calculations. Figure 2(b) shows that the bulk modulus depends weakly on the Hubbard on-site repulsion in the range of U_{eff} = 1–6 eV, and the values are all close to the CSM one. With further increasing U_{eff}, however, the bulk modulus decreases dramatically. At $U_{eff} \sim 6.5$ eV, the calculated value matches the experimental one (139.7 GPa). However, considering the uncertainty in the experimental determination of the bulk modulus [33], one would expect that the true value of B is somewhat larger (say around 150 GPa), thereby being consistent with the results for the lattice constant, for which the agreement between theory and experiment is achieved at $U_{eff} = 2$–3 eV.

As shown in figure 2(a), the lattice constant increases on going from the CSM to the VSM (with U_{eff} = 0 eV) treatment of the Lu 4f electrons, and then decreases with increasing Hubbard on-site Coulomb repulsion in the range of U_{eff} = 0–8 eV. These behaviors are rarely observed in usual DFT calculations. For example, in the DFT calculations on A-type Ce_2O_3, the lattice constant decreases on going from the CSM to the VSM, and then increases with increasing U_{eff}. The former behavior has been briefly explained by Hay *et al* [13] in terms of the (attractive) bonding interactions between the Ce 4f and O 2p electrons, which tends to shrink the lattice. Actually, the latter behavior with increasing U_{eff} could be also interpreted based on the same reasoning: with increasing on-site Coulomb interaction, the Ce 4f–O 2p band gap increases (see, for example, [21]) and thus the bonding interaction decreases. In the present case of Lu_2O_3, however, the variation of the calculated lattice constant using the CSM and VSM (U_{eff} = 0–8 eV) can only be interpreted in terms of the repulsive interaction between Lu 4f electrons and O 2p electrons. Intuitively, one would expect the Lu 4f orbitals and O 2p orbitals not to be bonded to each other in view of the closed 4f shell and the localized nature of the 4f orbital in the Lu atom. The quantum-mechanical theory of the valence bond for molecules [34] gives an approximate energy expression that contains single exchange integrals between bonded orbitals and also between orbitals not bonded to each other. The former exchange integrals corresponds to attraction and bond formation, and the latter integrals corresponds to repulsion, the magnitude of which decreases with decreasing overlap between the two orbitals. In Lu_2O_3, the well-known insufficient cancelation of self-interaction in the GGA (PBE) functional overestimates the Lu 4f eigenvalues and thus places the 4f orbitals in the same energy region as the O 2p orbitals (as shown later), giving rise to a strong overlap between the two types of orbitals. This spurious overlap leads to strong repulsive interactions between Lu 4f electrons and O 2p electrons. By including a Hubbard on-site repulsion term to reduce the remaining self-interaction, the 4f one-electron energies are shifted towards lower energies. The Lu 4f–O 2p orbital overlap is then reduced and the repulsion is decreased, leading to shrinkage of the crystal. This shrinkage becomes more dramatic when the crystal volume is reduced, as shown in figure 2(a).

3.2. Electronic properties

The structural behaviors in figure 2 are closely correlated to the electronic structure of Lu_2O_3. Figure 3 plots the orbital-projected density of states (DOSs) for Lu_2O_3 calculated within the VSM, where the Fermi energy E_F has been set to be zero. Three values of U_{eff} = 0, 5, and 8 eV have been chosen in order to show the variation of DOS with respect to increasing U_{eff}. One can see that, except for the Lu 4f band, the energy positions of the O 2s, 2p, and Lu 5d bands in figures 3(a)–(c) are all similar. The O 2s band lies at about 16 eV below the Fermi level. The O 2p states form a band of 4.4 eV wide just below the Fermi level, while the Lu 5d states constitutes a conduction band lying 4.0–5.0 eV above E_F, which are all smaller than the value 5.8 ± 0.1 eV observed experimentally [9]. This underestimation can be traced to the well-known shortcomings of the GGA. Figure 3(a) shows that, without accounting for the strong on-site Coulomb repulsion among the localized 4f electrons (U_{eff} = 0 eV), the 4f states are situated in the same energy region as the O 2p states in the vicinity of the Fermi level, with strong 4f–2p hybridization. A further indication of this hybridization can be observed from the similar position of the peak at −2.8 eV between the Lu 4f

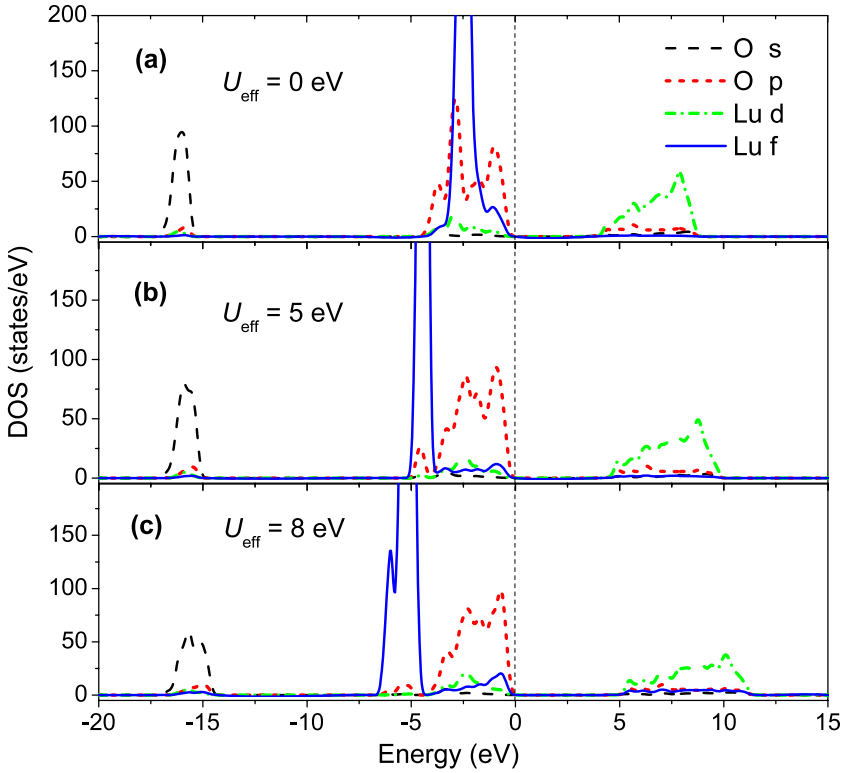

Figure 3. Orbital-projected densities of states of Lu_2O_3 calculated at the PBE + U level with (a) $U_{eff} = 0$ eV, (b) $U_{eff} = 5$ eV, and (c) $U_{eff} = 8$ eV, using the respective optimized structures. The Fermi level is set as zero energy.

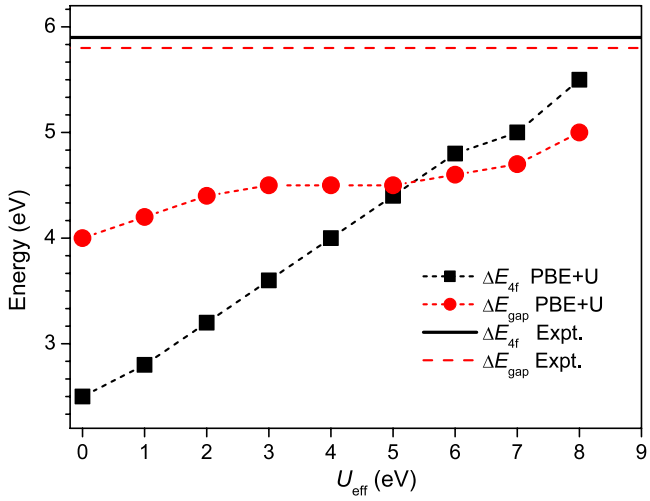

Figure 4. Variations of the 4f band (ΔE_{4f}) and 5d band edge (ΔE_{gap}) positions with respect to increasing U_{eff} calculated using the respective optimized structures. The corresponding experimental values are also shown for comparison.

and O 2p bands. As discussed above, the occurrence of 4f and 2p states in the same energy window is mainly due to the incomplete self-interaction cancelation of the 4f electrons in the PBE functional, which overestimates the Lu 4f one-electron energies. With introduction of a Hubbard on-site repulsion term to correct for the self-interaction error, the 4f band is shifted downwards in energy, and when the parameter $U_{eff} = 5$ eV, a gap opens up between 4f and 2p bands, see figure 3(b). Further increasing U_{eff} shifts the 4f band to lower energies, and at $U_{eff} = 8$ eV (figure 3(c)) the 4f band is about 5.6 eV below the Fermi level, which is very close to the experimental value of 5.9 ± 0.1 eV. A close look at the DOS of the 4f and 2p bands at $U_{eff} = 8$ eV still reveals slight hybridization between Lu 4f and O 2p states, which may partly be attributed to the nonorthogonality of the Lu 4f and O 2p orbitals in the DFT+U scheme employed here, which becomes more pronounced when the Lu–O distance is reduced. This phenomenon has been discussed in detail in the literature in relation to cerium dioxide [19, 20].

Figure 4 shows the variation of the 4f band position (ΔE_{4f}) relative to the Fermi level with respect to increasing U_{eff} from 0 to 8 eV. It is seen that the ΔE_{4f} increases nearly linearly from 2.5 to 5.6 eV. From this trend, one might expect the experimental value (5.9 eV) could be reached if U_{eff} were further increased to about 9 eV. Unfortunately, the converged solution could not be obtained for PBE + U ($U_{eff} = 9$ eV) calculations of small cell volumes. Also shown in the figure is the weak increase of the 5d band edge position (ΔE_{gap}) relative to the Fermi level (or the fundamental band gap) with increasing U_{eff}. This is presumably explained by the fact that, when U_{eff} is increased, the optimized Lu–O distance decreases (as indicated in figure 2(a)) and thus the Lu 5d–O 2p interaction becomes stronger, which pushes the empty 5d band to slightly higher energies.

The PBE + U results show that the electronic structure depends strongly on the strength of the Hubbard on-site

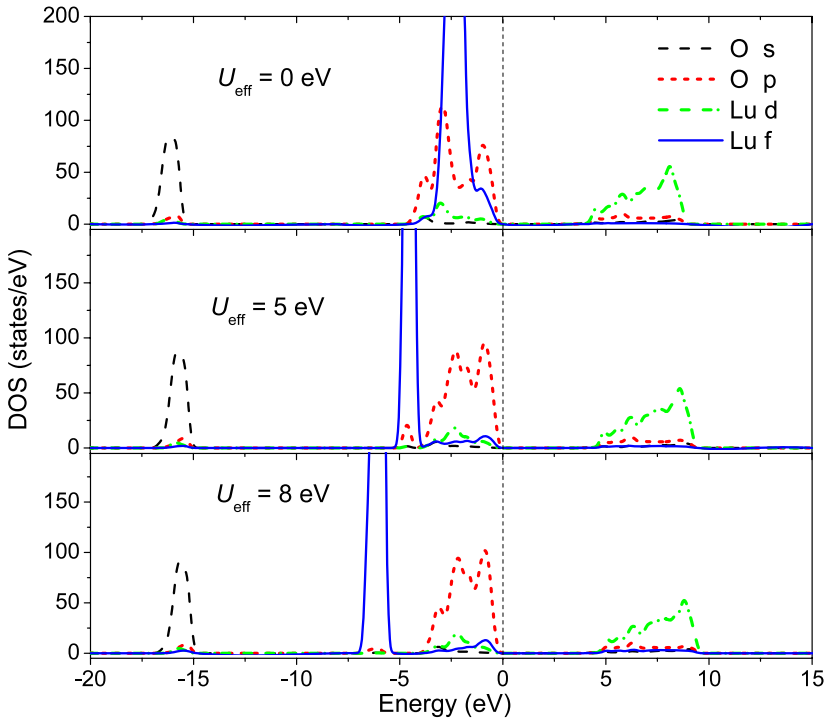

Figure 5. Orbital-projected densities of states of Lu_2O_3 calculated at the PBE + U level with (a) $U_{eff} = 0$ eV, (b) $U_{eff} = 5$ eV, and (c) $U_{eff} = 8$ eV, using the structure obtained with Lu 4f electrons frozen in the core. The Fermi level is set as zero energy.

Coulomb interaction. A small change of the interaction parameter U_{eff} leads to a substantial shift of the Lu 4f band with respect to the Fermi level. A value of around 8–9 eV for U_{eff} would be needed for a proper description of the 4f electronic structure. However, as discussed in section 3.1, a much lower value of U_{eff} = 2–3 eV is already sufficient for a good agreement between the theoretical and experimental lattice constant. Therefore, the large value of U_{eff} required to reproduce the experimentally observed 4f band position spoils the agreement for the structural properties. We recall also that the PBE result within the CSM gives a lattice constant in good agreement with the experimental value, see table 1. Although this agreement might be fortuitous in view of the fact that the GGA tends to overestimate the lattice constant while, on the contrary, the CSM reduces it by excluding the repulsion between Lu 4f and O 2p electrons, it is still interesting to see how the electronic structure evolves with increasing U_{eff} when using the CSM structure. Figure 5 plots the orbital-projected DOS for the cases of $U_{eff} = 0$, 5, and 8 eV predicted using this structure. Similar to the DOSs using the respective optimized structures (figure 3), the 4f band moves downwards with respect to the Fermi level with increasing U_{eff}. However, a notable difference (comparing figures 5(c) and 3(c)) is that the 4f band is now well separated (by ∼1.3 eV) from the valence 2p band at U_{eff} = 8 eV, which appears to be more physical. In figure 6 we plot the variation of 4f band position (ΔE_{4f}) relative to the Fermi level as a function of U_{eff} from 0 to 9 eV. The ΔE_{4f} increases linearly with increasing U_{eff} and at around $U_{eff} = 8$ eV, the experimental value is reached. The figure also shows that the fundamental band gap (ΔE_{gap}) is almost invariant with respect to increasing U_{eff}, as expected. Based on these observations, we suggest that, for Lu_2O_3 and

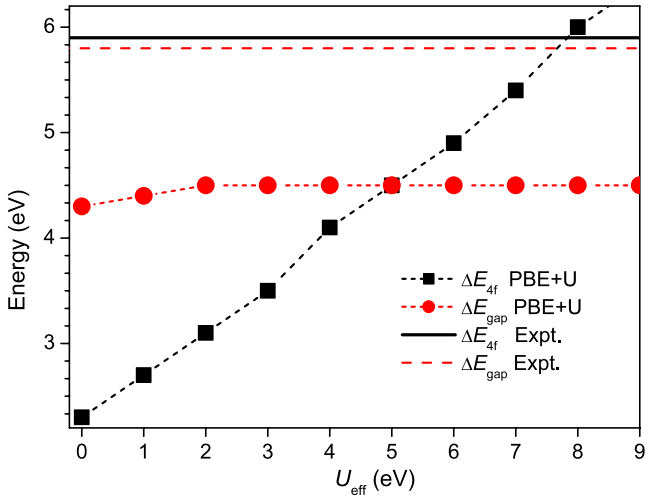

Figure 6. Variations of the 4f band (ΔE_{4f}) and 5d band edge (ΔE_{gap}) positions with respect to increasing U_{eff} calculated using the structure obtained with Lu 4f electrons incorporated in the core. The corresponding experimental values are also shown for comparison.

the related materials in cases where the 4f electronic properties of Lu are relevant, a practical calculational scheme could be that the structure is determined with the PBE functional with f electrons kept frozen in the core and then, using this structure, the electronic properties are calculated by the PBE + U approach with a value of U_{eff} around 8 eV.

4. Conclusions

In the present work, we have investigated the structural and electronic properties of the C-type Lu_2O_3 crystal using the

periodic DFT. The closed-shell Lu 4f electrons have been considered within two models (the CSM and the VSM), in which the f electrons were treated as part of the core and as valence electrons, respectively. In the latter model the PBE + U approach has been used to account for the strong correlation associated with the 4f electrons. We found that within the CSM the PBE calculation gave a lattice constant in good agreement with experiment whereas within the VSM the agreement is only moderate. With inclusion of the Hubbard on-site term for the 4f electrons within the VSM, the calculated and experimental lattice constants agree well at $U_{\text{eff}} = 2$–3 eV. However, for the 4f electronic structure, the best agreement is only achieved at a much higher value of U_{eff}, being in the range of 8–9 eV. This indicates that good agreement between theory and experiments for both structural and electronic properties of Lu_2O_3 could not be achieved with a single value of U_{eff}. The dependences of the properties with respect to increasing U_{eff} have also been examined. An interesting observation is that the lattice constant increases when extracting the 4f electrons from the core to the valence in the PBE calculations, and decreases with increasing U_{eff} in the PBE + U calculations. This observation, which is rare in the usual DFT calculations for lanthanide oxides, has been explained in terms of the repulsive interaction between Lu 4f and O 2p electrons arising from the incomplete cancelation of the self-interaction among the localized 4f electrons. Finally, a practical calculational scheme in the DFT + U framework has been proposed for Lu_2O_3 and the related materials where the 4f electronic properties are important; that is, structures are optimized using the GGA (PBE) functional within the CSM, and based on these structures the electronic properties are then investigated.

Acknowledgments

This work was supported by the NSFC (Grant Nos 10804001, 10674002 and 20773024), National 863 projects (Grant No. 2006AA09Z243-3), and Program for Innovative Research Team in Anhui Normal University of China.

References

[1] Haire R G and Eyring L 1994 *Handbook on the Physics and Chemistry of Rare Earths* vol 18, ed K A Gschneidner Jr, L Eyring, G R Choppin and G R Lande (Amsterdam: Elsevier) pp 413–506
[2] Jia G, Zheng Y, Liu K, Song Y, You H and Zhang H 2009 *J. Phys. Chem.* C **113** 153
[3] Yang J, Zhang C, Peng C, Li C, Wang L, Chai R and Lin J 2009 *Chem.—Eur. J.* **15** 4649
[4] Yang J, Li C, Quan Z, Zhang C, Yang P, Li Y, Yu C and Lin J 2008 *J. Phys. Chem.* C **112** 12777
[5] Trojan-Piegza J, Niittykoski J, Hölsä J and Zych E 2008 *Chem. Mater.* **20** 2252
[6] Sokolnicki J 2007 *J. Solid State Chem.* **180** 2400
[7] Qi Z, Liu M, Chen Y, Zhang G, Xu M, Shi C, Zhang W, Yin M and Xie Y 2007 *J. Phys. Chem.* C **111** 1945
[8] Zych E 2002 *J. Phys.: Condens. Matter* **14** 5637
[9] Perego M, Seguini G, Scarel G and Fanciulli M 2006 *Surf. Interface Anal.* **38** 494
[10] Seguini G, Bonera E, Spiga S, Scarel G and Fanciulli M 2004 *Appl. Phys. Lett.* **85** 5316
[11] Wu B, Zinkevich M, Aldinger F, Wen D and Chen L 2007 *J. Solid State Chem.* **180** 3280
[12] Hirosaki N, Ogata S and Kocer C 2003 *J. Alloys Compounds* **351** 31
[13] Hay P J, Martin R L, Uddin J and Scuseria G E 2006 *J. Chem. Phys.* **125** 034712
[14] Da Silva J L F, Ganduglia-Pirovano M V, Sauer J, Bayer V and Kresse G 2007 *Phys. Rev.* B **75** 045121
[15] Anisimov V I, Zaanen J and Andersen O K 1991 *Phys. Rev.* B **44** 943
[16] Anisimov V I, Solovyev I V, Korotin M A, Czyżyk M T and Sawatzky G A 1993 *Phys. Rev.* B **48** 16929
[17] Solovyev I V, Dederichs P H and Anisimov V I 1994 *Phys. Rev.* B **50** 16861
[18] Jiang Y, Adams J B and van Schilfgaarde M 2005 *J. Chem. Phys.* **123** 064701
[19] Fabris S, de Gironcoli S, Baroni S, Vicario G and Balducci G 2005 *Phys. Rev.* B **71** 041102
[20] Andersson D A, Simak S I, Johansson B, Abrikosov I A and Skorodumova N V 2007 *Phys. Rev.* B **75** 035109
[21] Loschen C, Carrasco J, Neyman K M and Illas F 2007 *Phys. Rev.* B **75** 035115
[22] Tran F, Schweifer J, Blaha P and Schwarz K 2008 *Phys. Rev.* B **77** 085123
[23] Temmerman W M, Petit L, Svane A, Szotek Z, Lüders M, Strange P, Staunton J B, Hughes I D and Gyorffy B L 2009 *Handbook on the Physics and Chemistry of Rare Earths* vol 39, ed K A Gschneider Jr, J-C G Bünzli and V K Pecharsky (Amsterdam: Elsevier) pp 1–112
[24] Kresse G and Furthmüller J 1996 *Phys. Rev.* B **54** 11169
[25] Blöchl P E 1994 *Phys. Rev.* B **50** 17953
[26] Kresse G and Joubert D 1999 *Phys. Rev.* B **59** 1758
[27] Perdew P, Burke K and Ernzerhof M 1996 *Phys. Rev. Lett.* **77** 3865
[28] Dudarev S L, Botton G A, Savrasov S Y, Humphreys C J and Sutton A P 1998 *Phys. Rev.* B **57** 1505
[29] Hafner J 2008 *J. Comput. Chem.* **2044** 29
[30] Bartos A, Lieb K P, Uhrmacher M and Wiarda D 1993 *Acta Crystallogr.* B **49** 165
[31] Murnaghan F D 1944 *Proc. Natl Acad. Sci.* **30** 244–7
[32] Birch F 1947 *Phys. Rev.* **71** 809
[33] Manning W R and Hunter O Jr 1970 *J. Am. Ceram. Soc.* **53** 279
[34] Slater J C 1931 *Phys. Rev.* **38** 1109